

# STUDY OF ABNORMAL HEAT TRANSFER DURING FORCED AND NATURAL CONVECTION SCENARIOS IN A PRISMATIC CORE OF A VHTR: NUMERICAL AND EXPERIMENTAL RESULTS

Francisco I. Valentín<sup>a</sup>, Narbeh Artoun<sup>a</sup>, Ryan Anderson<sup>b</sup> and Masahiro Kawaji<sup>a,c,\*</sup>

<sup>a</sup>City College of New York

<sup>b</sup>Montana State University

<sup>c</sup>The CUNY Energy Institute

[fivalente@gmail.com](mailto:fivalente@gmail.com); [narbeh.artoun@gmail.com](mailto:narbeh.artoun@gmail.com); [ryan.anderson@coe.montana.edu](mailto:ryan.anderson@coe.montana.edu);

\*Corresponding Author: [kawaji@me.ccnycunyu.edu](mailto:kawaji@me.ccnycunyu.edu)

## ABSTRACT

Very High Temperature Reactors (VHTRs) are one of the Generation IV gas-cooled reactor models proposed for implementation in next generation nuclear power plants. A high temperature/pressure test facility for forced and natural circulation experiments has been constructed. This test facility consists of a single flow channel in a 2.7 m (9') long graphite column equipped with four 2.3kW heaters. Extensive 3D numerical modeling provides a detailed analysis of the thermalhydraulic behavior under steady-state, transient, and accident scenarios. In addition, forced convection experiments with air and nitrogen were conducted for inlet Reynolds numbers from 1,500 to 70,000. Numerical results, using commercial finite element package, COMSOL Multiphysics, were validated with forced convection data displaying maximum percentage errors under 15%. Based on this agreement, simulations are also extended to study natural circulation of nitrogen and helium between two connected vessels, resembling the behavior between inner and outer cooling channels in a VHTR reactor core. Results were obtained for Rayleigh numbers of  $\sim 10^6$ . This work also examines flow laminarization for a full range of Reynolds numbers including laminar, transition and turbulent flow under forced convection and natural circulation and its impact on heat transfer under various scenarios to examine the thermal-hydraulic phenomena that could occur during both normal operation and accident conditions.

## KEYWORDS

Forced convection, heat transfer, VHTR, high temperature gas reactor

## 1. BACKGROUND

Very High Temperature Reactors (VHTRs) are one of the Generation IV reactors that have been proposed for DOE's Next Generation Nuclear Plant. Several characteristics have stimulated this development including higher efficiencies due to higher working temperatures and the additional benefits of passive safety systems including intracore conduction and natural circulation for decay heat removal and dissipation in accident scenarios. Key phenomena have also been identified as leading to localized hot spots in the nuclear reactor, including: degraded heat transfer in coolant channels, laminarization of flow, effects of bypass flow, and non-uniform heat generation across the core.<sup>[1-2]</sup>

One issue in studying flow laminarization is implementing applicable turbulence models with appropriate parameters. Mikielewics et al.<sup>[3]</sup> successfully studied internal velocity and temperature fields of strongly heated internal flows numerically. They examined eleven turbulence models, requiring two partial differential equations or less. They concluded that the model by Launder<sup>[4]</sup> performed best in predicting experimental data.<sup>[3]</sup> Their study highlights the difficulty involved in modeling even simple axisymmetric gas flows in pipes subjected to intense heating, which take into account variable gas properties since only one out of the eleven models agreed on heat transfer parameters such as the Nusselt number. Several of these other  $k-\epsilon$  models specifically developed for low Reynolds number applications even gave unacceptably high Nusselt number predictions.<sup>[3]</sup> In addition, many of these studies were specific to the conditions used in the experiments of Shehata and McEligot.<sup>[5,6]</sup>, thus the knowledge base available outside the conditions used in Shehata and McEligot's experiments is limited. This points to the limited range of applications of even the successful models, since their validation data was constrained to small tubes, low

gas densities, and/or microgravity applications so buoyancy effects were not important (situations representing dominant forced convection). These knowledge gaps, as they apply to VHTRs, are addressed in this paper.

In order to target these knowledge gaps, and to provide thermal-hydraulic data for code validation, a high pressure/high temperature test facility rated at 70 bar/923.15 K, has been constructed at City College of New York for conducting forced and natural convection heat transfer experiments with helium, nitrogen and air. This experimental facility consists of a pressure vessel which contains a 2.7 m (9') graphite column with four 2.3kW heaters symmetrically placed around a central coolant channel of 16.8 mm diameter. The objectives of this project are 1) to conduct experiments and obtain heat transfer data under various scenarios for validation of VHTR design and safety analysis codes, and 2) to examine the thermohydraulic phenomena that could occur during normal operation and accident conditions.

## 2. DESCRIPTION OF WORK

The present study addresses forced convection heat transfer, natural circulation flow and a flow laminarization phenomenon. Experimental data on forced convection heat transfer are presented for air and nitrogen, as well as natural circulation of helium. Furthermore, 3-dimensional numerical simulations are presented together with model validation based on experimental data and comparison to existing empirical correlations. The flow laminarization phenomenon is analyzed with regards to its general effect on heat transfer in the coolant channel using Reynolds, Nusselt, and Prandtl numbers, as well as non-dimensional buoyancy and acceleration parameters. The experimental conditions varied were the system pressure, heater power level, and volumetric flow rate.

Flow laminarization is one of the phenomena known to be closely connected to degraded heat transfer. Gas viscosity increases with temperature within reactor cooling channels, causing a reduction in the Reynolds number which can trigger flow laminarization when the incoming flow is just above the critical Reynolds number. On the other hand, the laminar flow can transition to turbulent flow when the gas is cooled in the downcomer channels under natural circulation. Natural circulation simulations are presented under Pressurized Conduction Cooldown (PCC) and Depressurized Conduction Cooldown (DCC). Under PCC and DCC, a radial temperature gradient would exist between the hot fuel and outer reflector regions of a VHTR core. Natural circulation of the coolant between the upper and lower plenums is investigated using a CFD model for natural circulation between two adjacent flow channels in this study. Many forced convection and natural circulation experiments have been conducted to provide detailed flow and heat transfer data which are being used to validate the CFD model and investigate turbulence parameters.

## 3. EXPERIMENTAL SETUP

Numerical simulations guided the test facility design based on maximum permitted temperatures and pressure induced stresses in the pressure vessel. A detailed analysis of reactor conditions included steady-state and transient operations and accident scenarios for a VHTR. The details of the forced convection experimental setup have been previously described.<sup>[7]</sup> Figure 1 shows a schematic diagram for natural circulation experiments. Both pressure vessels had an inner diameter of 16.8 mm and contained identical graphite test sections which were 2.74 m (9-ft) long and 106.7 mm

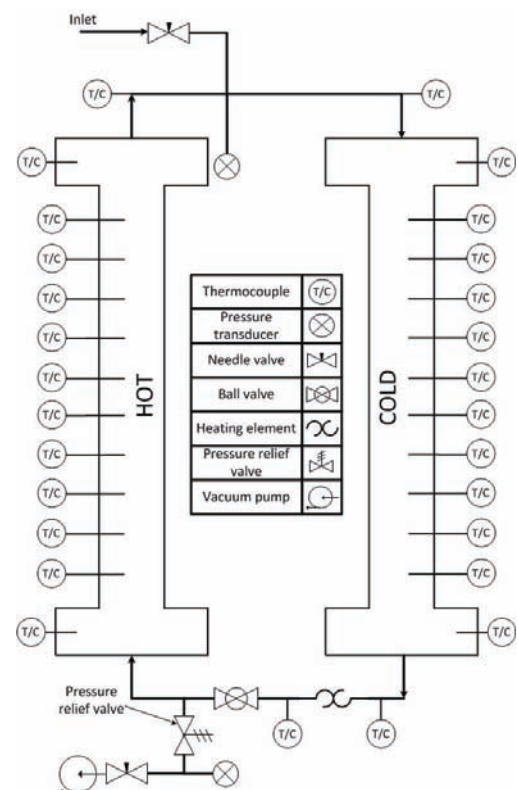


**Fig. 1 Schematic diagram of natural circulation experiment setup**

(4.25-inch) in outer diameter. Low thermal conductivity insulation ( $k = 0.05\text{-}0.3 \text{ W/mK}$ ) provided thermal insulation between the graphite column and the inner surface of the pressure vessel. Inserted into the graphite column are four 12.7 mm (0.5") diameter heater rods each rated at 2.3kW. Lastly, a circular 16.8 mm diameter coolant channel is drilled through the center axis of the graphite column to allow the coolant gas to flow through. The two graphite flow channels were connected at the top and bottom to form a closed flow loop. In the natural circulation (NC) experiments, the hot vessel (HV) was heated while the heaters in the cold vessel (CV) were turned off. These NC experiments covered a range of pressure from 6 to 64 bar (100 to 940 psi), and graphite temperature ranging from 373 to 773 K.

#### 4. SIMULATION MODEL

Figure 2 (a-c) presents the model geometry used featuring multidimensional conduction within all solid domains and convective heat removal by a gas flowing through the graphite column at various flow rates. Fig. 2-a displays the geometry used for forced convection simulations, whereas Fig. 2-b shows the union of two test sections for natural circulation experiments and simulation. In the present work, forced convection results are presented with air as the working fluid for comparison of numerical and experimental results. PCC and DCC simulations used either nitrogen or helium as the working fluid. The different domains near the top flange of each pressure vessel are also shown in Fig.2-c.

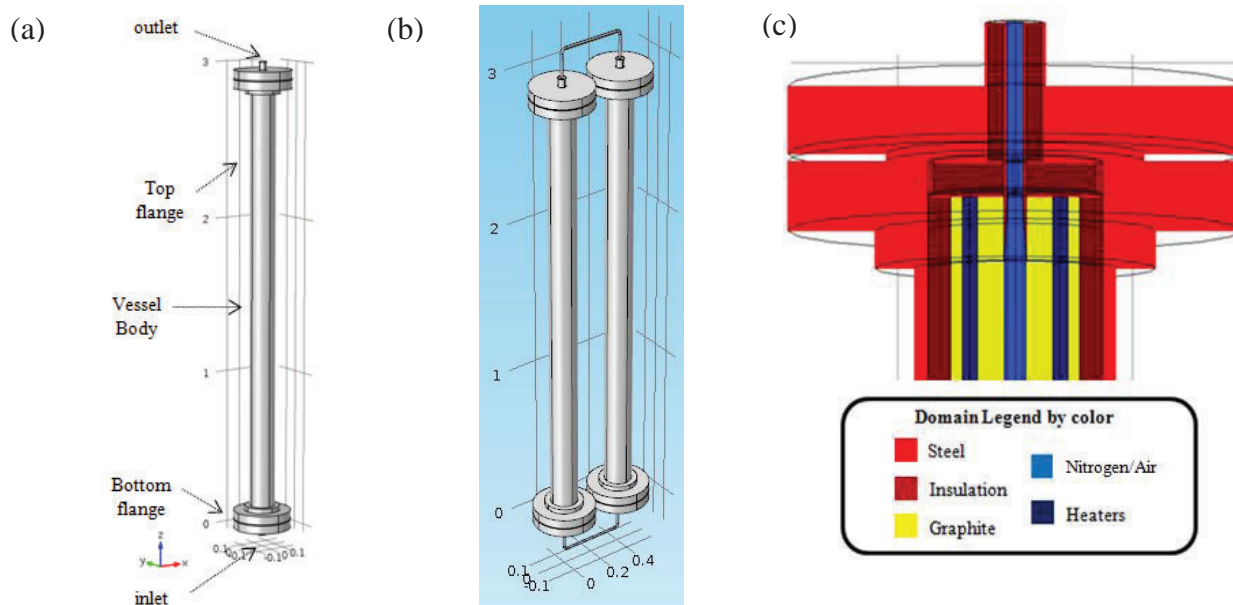


**Figure 2 Simulation model geometry and domains**

In the CFD simulation, continuity and momentum equations are solved to describe the behavior of the fluid subjected to a pressure gradient, where the fluid properties are temperature and pressure dependent.<sup>[8]</sup>

$$\nabla \cdot (\rho \bar{u}) = 0 \quad (1)$$

$$\rho (\bar{u} \cdot \nabla) \bar{u} = \nabla \cdot \left[ -p \bar{I} + (\mu + \mu_T) (\nabla \bar{u} + (\nabla \bar{u})^T) \right] - \frac{2}{3} (\mu + \mu_T) (\nabla \cdot \bar{u}) \bar{I} + \bar{F} \quad (2)$$

In Eqs. 1 and 2,  $\bar{u}$  represents the velocity vector of the fluid,  $\rho$  is the fluid density,  $p$  is the absolute pressure and  $\bar{F}$  refers to the body force, which is defined as  $\bar{F}_z = -\rho g$ . The energy equation is given by:

$$\rho c_p \bar{u} \cdot \nabla T = \nabla \cdot (k \nabla T) + Q \quad (3)$$

where  $c_p$ ,  $k$ ,  $Q$ , and  $T$  are heat capacity, thermal conductivity, volumetric heat source and temperature, respectively. Thermal conductivity and  $c_p$  are given as functions of temperature.

#### 4.1 Numerical Procedure

A 3D model was constructed and analyzed using the COMSOL Multiphysics code.<sup>[8]</sup> A non-isothermal fluid flow module was used, which provided coupling between momentum and energy equations. The fluid was modeled with a RANS  $k-\varepsilon$  turbulence model for forced convection simulations. For natural circulation simulations, the fluid was modeled using a laminar flow model. Differences in the results between modeled fluid types will be addressed in the discussion.

Model assumptions are as follows:

- 1) For forced convection simulations, the fluid is treated as an ideal gas, and
- 2) The coolant is transparent to radiation inside the cooling channel.

In the present work, due to the large density variations within the fluid caused by large temperature variations obtained through a scaling analysis, the Boussinesq approximation was not invoked. Because of this, the present model for natural circulation treats the fluid as a real gas.

#### 4.2 Boundary Conditions

Fluid velocity and temperature are specified at the inlet, thus allowing for the calculations of pressure and density, therefore setting the inlet Reynolds number. At the outlet, a convection dominated boundary condition is specified. The temperature gradient in the normal condition is zero and radiative heat transport is neglected. This is usually a good approximation of the conditions at an outlet boundary in a heat transfer model with fluid flow.<sup>[8]</sup> Working pressure is established by defining the pressure at the outlet. In all boundaries surrounding the vessel, natural convection and radiation heat losses are specified with a surface emissivity,  $\varepsilon$ , of 0.4.<sup>[9]</sup> Natural convection heat transfer coefficients are calculated from known correlations for vertical and horizontal plates whose length and hydraulic diameter are user specified.<sup>[10]</sup>

Natural circulation simulations utilized similar boundary conditions, with the exception of those defined at the outlet and inlet. For these simulations, a pressure constraint point was defined at the outlet of the heated channel, thus establishing overall working pressure. In addition, in order to allow for transport of heat between vessels, interconnecting tubes are insulated.

#### 4.2 Mesh Selection

A mesh refinement analysis was carried out. The chosen convergence parameters were the average temperature and velocity of the fluid in the cooling channel within the graphite. The chosen mesh consisting of  $1.7 \times 10^6$  tetrahedral elements displayed less than 2% differences in average temperature and average velocity magnitude in reference to a finer mesh with  $2.7 \times 10^6$  elements. Due to the small differences, the coarser mesh was chosen to avoid high computational cost while still maintaining the desired precision. A similar meshing scheme was also used for DCC and PCC simulations, involving a total  $3.95 \times 10^6$  elements.

### 5. RESULTS AND DISCUSSION

Forced convection experiments were conducted with air and nitrogen at various flow rates (30-600 SLPM). The data presented in this paper cover 30 experiments carried out with air and 30 experiments with nitrogen<sup>[7]</sup>. Figure 3 shows the temperatures measured in the graphite test section in one of the air forced convection experiments. After the heater power was turned on at  $t = 0$  and gas flow started at  $t = 2,000$  s, the graphite temperatures at ten different elevations gradually changed and reached near steady state values after about 3 hours. The temperature increased with the elevation since the gas entering the test section at the bottom was at room temperature. The error bars in the inset indicate the range of temperatures measured at four radial locations in the same plane. The forced convection experiments were performed at different pressures from 1 to 70 bar, various flow rates (30-600 SLPM), and heater input power up to 6.4 kW. Flow regimes included turbulent, transition and laminar flows, over a wide range of Reynolds numbers from 1,500 to 70,000.

The method with which experimental and numerical data have been analyzed is now presented. More details can also be found in Valentin et al.<sup>[11]</sup> The graphite temperature data were analyzed for the last 30 seconds of the experiment when the change in any of the temperatures was less than 3°C per hour, a near steady state condition. The graphite flow channel was divided into eleven sections, and an energy balance was performed for each segment. As given by Eq. 4, the local energy balance for the  $i_{th}$  segment included energy generated by the heaters ( $Q_{gen\_i}$ ), net axial heat conduction in both the graphite and pressure vessel wall,  $Q_{net\_axial\_cond\_i}$ , given by Eq. 5, heat loss from the pressure vessel's outer surface,  $Q_{HL\_i}$ , and heat transfer to the fluid,  $Q_{fluid\_i}$ .

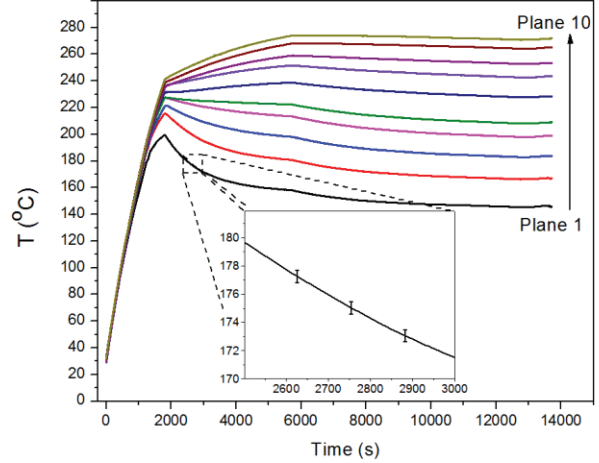


**Fig. 3 Typical graphite temperature data for air at 23.8 bar and 614 SLPM**

$$Q_{HL\_i} + Q_{net\_axial\_cond\_i} + Q_{fluid\_i} = Q_{gen\_i} \quad (4)$$

$$Q_{net\_axial\_cond\_i} = Q_{axial\_cond\_PV\_i} + Q_{axial\_cond\_graphite\_i} \quad (5)$$

The net axial conduction in the PV wall and graphite was calculated from the measured axial temperature profiles. Heat loss data were obtained in separate tests with a stagnant gas, so that the heat transfer to the fluid was set equal to zero in the heat balance. The heat loss data were then correlated with the average PV surface and graphite temperatures at different heater power levels. This correlation was then applied to forced convection tests in order to obtain the rate of heat transfer to the fluid.

By solving Eq. 4 for the local rate of heat transfer to the fluid,  $Q_{fluid\_i}$ , for the  $i_{th}$  segment, Eq. (6) can then be used to calculate the outlet bulk temperature,  $T_{i+1}$ , for the segment,  $i$ .

$$T_{i+1} = \frac{Q_{fluid\_i}}{\dot{m}c_{p\_i}} + T \quad (6)$$

The local Nusselt number was calculated from Eq. (7), where the thermal conductivity,  $k$ , was interpolated from a table of thermal conductivities for air and nitrogen as a function of temperature.<sup>[12]</sup>

$$Nu_i = \frac{h_i D}{k_i} \quad (7)$$

The local heat transfer coefficient was calculated from:

$$h_i = \frac{Q_{fluid\_i}}{(\pi D L_i)(T_{wall\_i} - T_{bulk\_i})} \quad (8)$$

where  $L_i$  is the length of each segment, 249.4 mm.

The local Reynolds number was calculated from Eq. (9) where  $u$ ,  $\rho$ ,  $\mu$ , represent local fluid velocity, density and dynamic viscosity, respectively.

$$Re_i = \frac{4\dot{m}}{\pi D \mu_i} = \frac{u_i D}{\nu_i} \quad (9)$$

The dynamic viscosity was calculated from Sutherland's formula, which can be used to derive the dynamic viscosity of an ideal gas as a function of temperature.<sup>[12]</sup>

Additional parameters were also calculated which will be presented further on in the discussion. Numerical results were analyzed in a similar manner to obtain local  $Nu$  and  $Re$  values along the channel.

## 5.1. Forced Convection Results

### 5.1.1 Model Validation: Experimental Results

Using the near steady state graphite temperature data and PV surface temperature data (not shown), the axial bulk temperature profile and local Nusselt and Reynolds numbers were calculated. Figure 4a and Fig. 4b present variations of the local Nusselt number with local Reynolds number for nine air and eight nitrogen experiments. Experimental uncertainties in the Reynolds and Nusselt numbers were estimated to be 3% and 5.3%, respectively. The results from six numerical simulations for air and seven simulations for nitrogen at different inlet Reynolds numbers are also shown. The numerical results appear discontinuous because one single simulation could not cover the whole desired Reynolds number range thus the discontinuities mark the commencing of a new set of numerical data. For a given Reynolds number, different values of Nusselt number might be expected depending on the local quantity of the wall-to-bulk temperature ratio,  $T_w/T_b$ . Numerical results for both air and nitrogen can be seen to cover larger ranges of Reynolds numbers than the experimental data because the maximum graphite temperatures in the simulations were allowed to reach higher values than in the experiments, thus the Reynolds number dropped to lower values in the simulations. On average, a 35% reduction in the Reynolds number was observed for air numerically as compared to an average of 29% experimentally. Nonetheless, good agreement within 15% can be observed between the numerical and experimental results compared in Fig. 4. The experimentally obtained Nusselt numbers for average Reynolds numbers less than  $10^4$  were within 7% of the numerical predictions with a standard deviation of 7%. The slight overprediction of the experimental data could be due to the effects of flow laminarization which will be discussed in the next section.

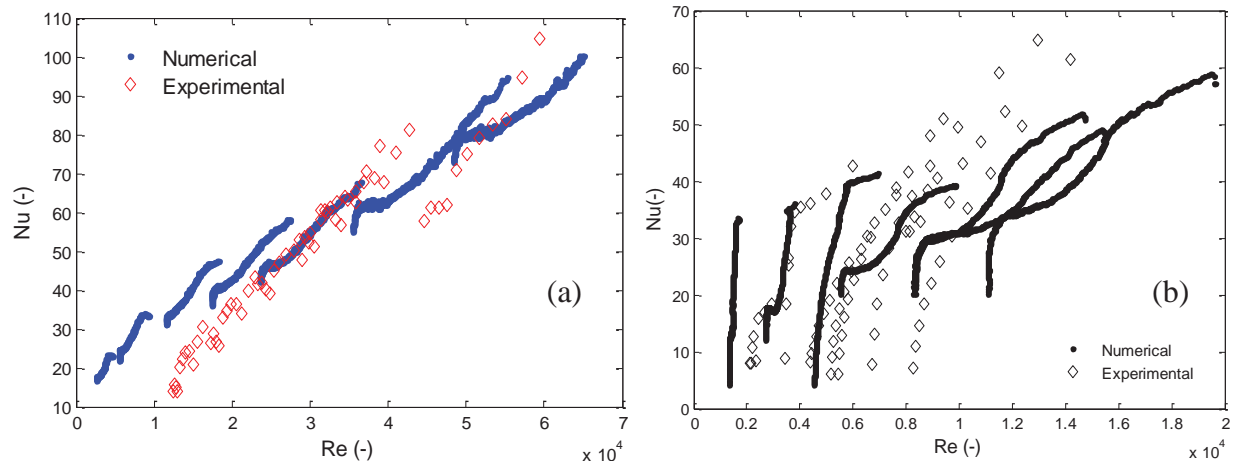


**Figure 4** Variations of local Nusselt number with local Reynolds number for a) air and b) nitrogen.

Several researchers<sup>[15]</sup> have concluded that the well-known and commonly used convective heat transfer correlations, Dittus-Boelter and Sieder-Tate, are not strictly applicable to VHTRs. However, several other groups recommended slight modifications of these correlations. In Fig. 6a, various correlations<sup>[13-20]</sup> for turbulent convection giving Nusselt number variations with the Reynolds number are compared with numerical simulation results. The following parameter values were assumed for the Nusselt number comparison:  $Pr = 0.665$ ,  $z/D=50-125$  (fully developed flow),  $T_{bf}/T_w$  is varied between 0.5 and 1, and  $Re = 15,000$  to  $60,000$ . Figure 6b plots the Nusselt numbers obtained from various correlations against the average Nusselt numbers obtained from the numerical simulations. Good agreement is found between the numerical predictions from the COMSOL simulations with the following correlations: McEligot<sup>[13]</sup>, Taylor<sup>[15,16]</sup>, and Travis and El-Genk<sup>[20]</sup>.

These results provide additional validation of our results, but they also show that for the same Reynolds number there is a wide range of possible Nusselt numbers given by different correlations. This means that every correlation may not be applicable to every physical situation. The use of these correlations will also mean that some very specific physical parameters, such as temperature gradient, have to be known a

priori; which might not likely be the case.

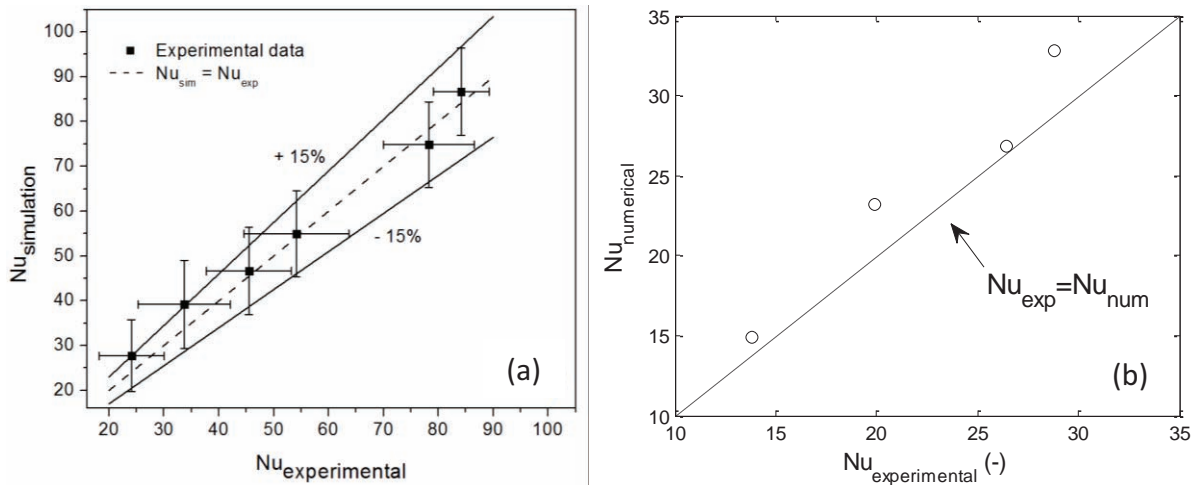


Figure 5 Comparison of experimentally obtained Nusselt numbers with numerical predictions for a) air demonstrating a maximum difference of 15%, and b) nitrogen.

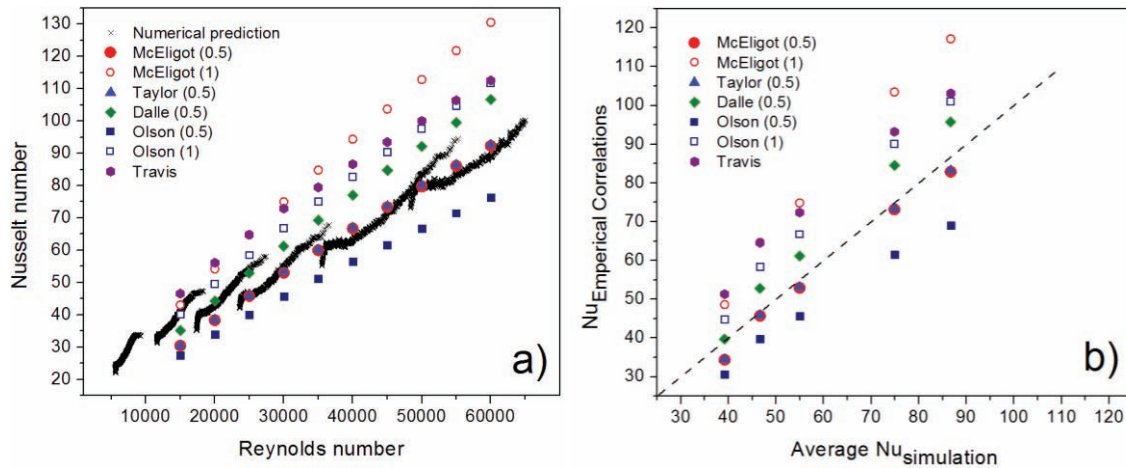


Figure 6 Comparison of numerical predictions with existing turbulent convection correlations: (a) local Nusselt number variation with local Reynolds number, and b) average Nusselt numbers

### 5.1.2 Forced Convection Heat Transfer at High Temperatures and Pressures

Based on the experimental-numerical simulation agreements above, additional core behavior and thermal-hydraulic phenomena are addressed. The remaining results discussed in this work belong to numerical results extracted from simulations. Temperature, pressure and velocity profiles in the graphite test section were predicted for air flows at different Reynolds numbers, system pressures, and heater power levels. The analyzed data include wall temperature, fluid bulk temperature, velocity, kinematic viscosity, Prandtl number and thermal conductivity in order to calculate the heat transfer coefficient in terms of Nusselt and Reynolds numbers. Figure 7a displays a typical plot of a temperature distribution in the  $y$ - $z$  plane with heat flux indicated by arrows. As can be observed, most of the heat generated by the heater rods is transferred to the fluid. Additionally, heat losses through the pressure vessel wall are seen all through the vessel sides, especially the upper flange.

The key phenomenon of interest to this study is flow laminarization, which could lead to degraded heat transfer in the core. Figure 8a displays the decrease in the Reynolds number as the air rises through the cooling channel at different pressures. Several factors play crucial roles in flow laminarization. Changes in fluid density do not cause major changes in fluid velocity. The Reynolds number reduction shown is a

viscosity dominated behavior since the fluid viscosity increases at a faster rate than the fluid velocity, thus leading to a decrease in the Reynolds number. Overall, a 35% drop in the Reynolds number was predicted for air. Therefore, turbulent flows at the inlet close to transition regions will traverse transitional zones and exit with laminar Reynolds numbers. In the numerical and experimental results presented, flows did not descend from fully turbulent to laminar flow due to the limited coolant channel length. Therefore, the flow regime transition is only observed from transitional to laminar flow. Understanding and obtaining data for this behavior is crucial for models intending to accurately predict this phenomenon.

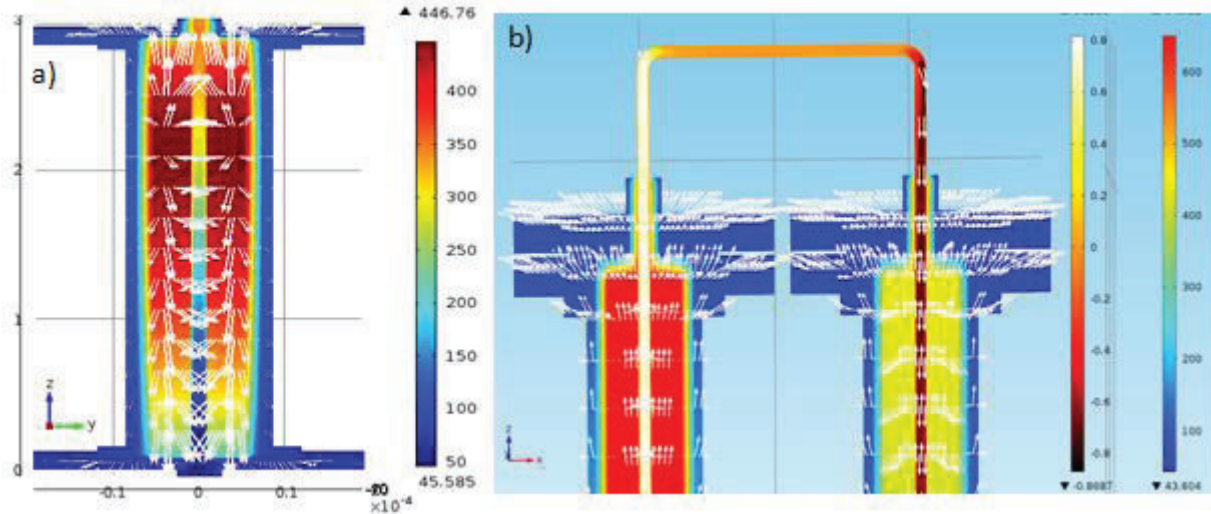


**Figure 7 a) Typical y-z temperature plot and heat flux indicated by arrows for inlet  $Re = 27,800$ , heat generation rate = 900 W, and  $p = 45$  bar. (The figure's aspect ratio is modified for visualization.) b) Top flange region temperature ( $^{\circ}C$ ) and velocity (m/s) profile at  $p = 60$  bar and heat generation rate = 3,275 W.**

Figure 8b is shown to highlight the effects of fluid property variations due to heating and their effect on both flow and thermal characteristics. The Reynolds number reduction in the axial direction is attributed to an increase in viscosity due to an increase in the bulk temperature ( $\mu \sim T^{0.7}$ ). Similarly, an increase in fluid thermal conductivity due to a gas temperature increase ( $k \sim T^{0.7}$ ), leads to decreasing Nusselt numbers. Although a slight increase in the heat transfer coefficient is expected ( $h \sim T^{0.24}$ ), which is seen in the figure, the downstream section dominated by the end effects experiences a drastic decrease in the heat transfer coefficient due to a large decrease in the wall heat flux.

Figure 9 shows the effects of the buoyancy parameter<sup>[21]</sup> ( $Bo^*$ ) and acceleration parameter<sup>[22]</sup> ( $K_v$ ), which are defined below, on the ratio of the numerically calculated Nusselt number to the value predicted by the modified Dittus-Boelter equation. Larger differences between the two values exist as both of these Nusselt numbers increase even in fully developed regions. This ratio is expected to be larger for developing flows in the entrance region. However, in simulations where the entrance values of these parameters were relatively low, fully developed flow regions yielded ratios closer to 1, except for the downstream regions close to the exit, where the Nusselt numbers dropped due to the end effects.

$$Bo^* \approx \frac{Gr_q}{Re^{3.425} Pr^{0.8}} \quad (10)$$

where

$$Gr_q = \frac{g\beta q_w D^4}{k\nu^2} \quad (11)$$

$$K_v \approx \frac{4q^+}{Re} \quad (12)$$

where

$$q^+ \approx \frac{\beta q_w''}{Gc_p} \quad (13)$$

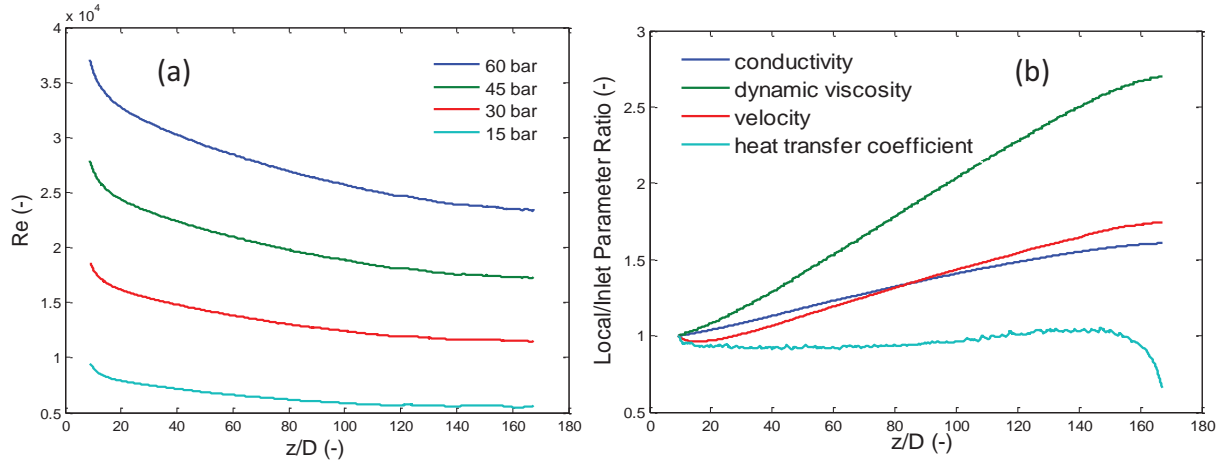


Figure 8 a) Axial variations of Reynolds number for air for fixed inlet velocity at different system pressures, and b) Local to inlet ratios of parameters used in Nusselt and Reynolds number calculations

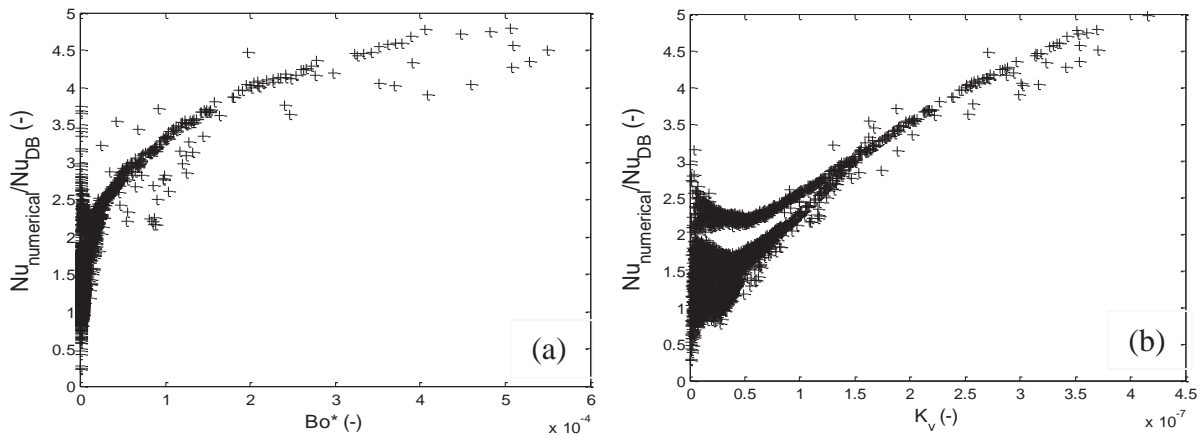


Figure 9 Compilation of five numerical runs for N<sub>2</sub> demonstrating higher deviation from Dittus-Boelter correlation (a) at higher Bo\* and (b) K<sub>v</sub> values.

### 5.1.3 Forced Convection at low Reynolds numbers (Re < 10,000): Flow Laminarization

Low Reynolds number flows, still above the transition zone where the Reynolds number drops after laminarization, are predicted to experience a characteristic behavior as shown in Fig. 10. These flows are generally slower and unable to remove a large amount of heat compared to higher Reynolds number flows. Consequently, the fluid bulk temperature will increase to a value equaling the wall temperature as shown in Fig. 10a. At a particular z location (point 3 in Fig. 10b), approximately 2.6 m below the outlet, the fluid bulk temperature reaches its maximum value. Beyond this point the fluid is unable to remove additional heat, and wall heat flux direction is reversed. This phenomenon has additional effects on the flow behavior since the buoyancy term,  $\bar{F}_z$ , no longer contributes to the increased fluid velocity. Points 1 and 5 are two vertical locations before and after the fluid has reached its maximum temperature. Points 2 and 4 are the points slightly before and after this maximum temperature at point 3.

The occurrence of the above behavior has been observed to affect the physics of the flow, such that heat flux direction is reversed if the gas temperature reaches a maximum value far from the inlet. The occurrence of this phenomenon was linked to the inlet buoyancy number as presented in Fig. 11. This figure plots the maximum buoyancy number, which occurs at the inlet of the coolant channel, against the location where the

maximum bulk temperature occurred. This location, moves further upstream, as the buoyancy number increases, meaning that the fluid is heated up to its maximum temperature sooner.

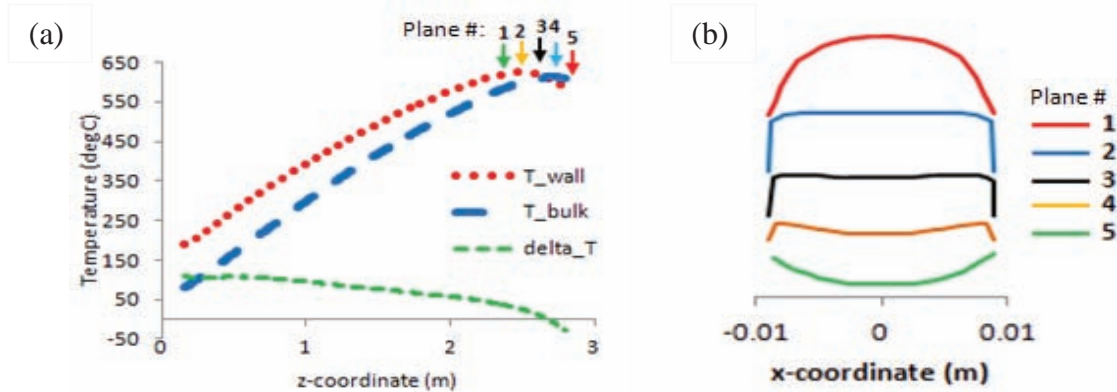


Figure 10 Variations of (a) wall and bulk fluid temperatures and temperature difference, and (b) fluid temperature profile for air at  $Re = 4,000$

## 5.2 Natural Circulation Results

For natural circulation experiments two different experimental schemes were used. In scheme 1 the electric heater rods were turned on in the HV at time  $t = 0$ . Natural circulation of the coolant was observed to occur immediately and after 6 ~ 7 hours, steady state was reached. The 2<sup>nd</sup> scheme consisted of turning on the heater power while the valve connecting the two test sections at the bottom (Fig. 1) was closed, thus not allowing any flow. After steady temperature profiles were reached in the heated test section, the valve was opened and natural circulation between the two vessels was initiated. Once again steady state was reached.

In order to measure the natural circulation flow rate, two 50W heating tapes [Chromalox, 121620] powered by a 24V DC source, were connected in parallel and placed around the interconnecting tube in the lower section (see Fig. 1). This tubing connecting the outlet of the cold vessel and inlet of HV was also insulated on the outer surface to minimize heat losses. A thermocouple was also installed at the insulation surface to measure the temperature difference between the insulation surface and ambient temperature in order to further corroborate any heat loss values. By applying power to the heating tape and measuring the inlet and outlet bulk temperatures at steady state, an energy balance given by Eq. (14) can be solved for two power levels to obtain the mass flow rate and the heat transfer coefficient for the insulation surface.

$$\dot{m}c_p(T_{out\_i} - T_{in\_i}) - h(T_{insulation\_i} - T_{ambient\_i}) = Q_{heater\_i} \quad (14)$$

### 5.2.1 Experimental Results

One of the VHTR's advantages over other new reactor designs is their capability to passively remove decay heat. This feature will enable long term cooling of these reactors without any forced convection or active cooling mechanisms. Such capability is due to effective surface cooling from the reactor vessel due to radiative heat transfer and natural convection. In addition, high thermal conductivity of graphite and natural circulation of coolant transport the decay heat from the core-region to the surface of the reactor vessel.

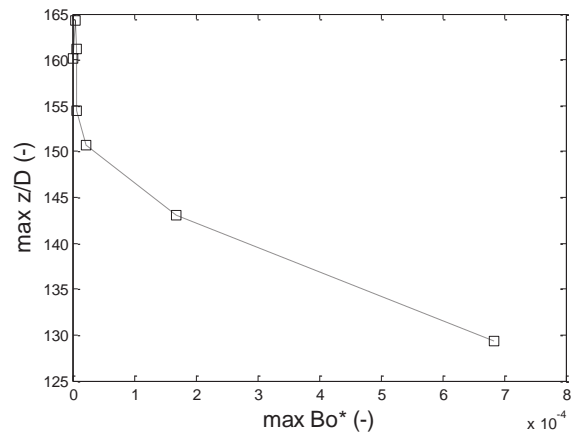
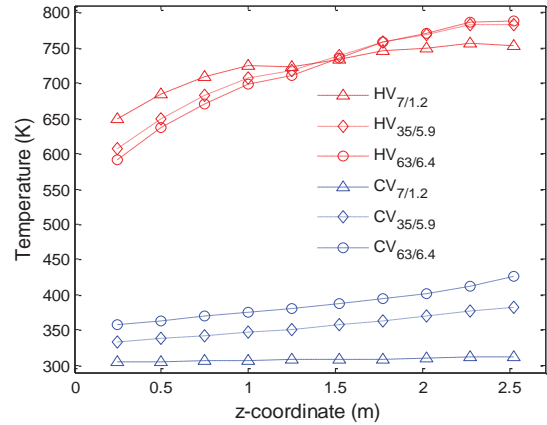


Fig. 11 Location of maximum bulk temperature against the maximum  $Bo^*$  number

Therefore, for safety analyses it is essential to study the reliability of such passive cooling systems.

In this section we present the results for natural circulation experiments which were carried out with helium at maximum hot vessel (HV) temperatures of 373 to 800 K and pressures ranging from 10 to 64 bar. In these experiments the effects of operating pressure and temperature on total dissipated heat were the objectives of this study. Figure 12 displays the results obtained at various pressures and heating rates in the hot vessel. The figure displays steady state temperature profiles, obtained through experimental scheme 1. The legend in the figure identifies the hot or cold vessel, followed by the operating pressure for that test, and finally the total heat dissipated by the closed flow loop in kilowatts. As observed there is higher heat quantity dissipated by the flow loop at higher pressures. The total amount of heat dissipated increases by a factor of nine as the pressure is increased by a factor of six.



**Fig. 12 Natural circulation tests (Scheme 1) for various pressures and the same graphite midpoint temperature.**

Figure 13 presents the measured temperature results for one test following the experimental scheme 2. The figure presents three test periods. The initial period is during the heating of the HV where natural circulation is prevented by a closed valve. In the second stage, the heater power is adjusted to reach steady state temperatures in the HV. The third stage allows for the occurrence of natural circulation by opening the valve until steady state is reached again. The total input power is maintained constant throughout the whole experiment. After the valve was opened, the average graphite temperature decreased by 363.15 K due to natural circulation cooling.

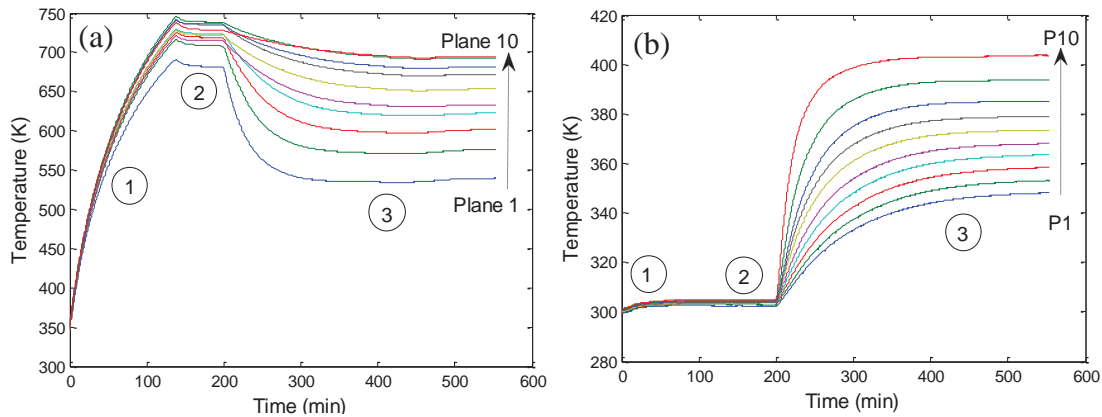


**Figure 13 Natural circulation test results for experimental scheme 2: a) graphite temperature variation at 10 planes in HV, b) graphite temperature variation in CV.**

### 5.2.2 Numerical Results

COMSOL simulation results for natural circulation of nitrogen are discussed in this section. The fractional role natural circulation is predicted to play in heat transport from the hot vessel to the cold vessel can be summarized in Table 1.

#### 5.2.2.1 Effect of Pressure

Simulations were extended to study natural circulation between two connected vessels, resembling the flow behavior between the coolant channels in the hot fuel zone and outer reflector zone in a VHTR core. Figure 14 displays predicted natural circulation of nitrogen under PCC conditions. This PCC case highlights 3.3 kW of total dissipated power while the graphite core was kept at a maximum temperature of 923 K. Due to

the small volume of the gas flowing through the two vessels, the rate of heat transport from the HV to CV was not a strong function of the system pressure.

This summary presents the system pressure, input heater power, total heat and fraction of heat dissipated from the HV by natural circulation. The amount of dissipated heat varied from 2.7 to 3.3 kW between 5 and 60 bar. In these simulations total heat input was varied, while maintaining a constant maximum graphite temperature of  $\approx 923\text{K}$ . As shown in Fig. 14, mass flux varied linearly with the working pressure, whereas, density increased with working pressure average velocity in the tubes decreased with increasing working pressure. As the mass flow rate increases, the temperature difference between hot and cold channels is reduced.

Of further interest is the study of flow and heat transfer behavior, especially the decreasing Reynolds number in the heated channel and increasing Re in the cooled channel. Figure 15a displays the passage of the fluid through the hot channel in the heated vessel representing the coolant channels in the “inner” fuel zone of the VHTR core and colder flow channels in the outer reflector zone. The outer channels act like a heat sink causing a downward fluid motion. While the heated channel causes a reduction in the Reynolds number, the colder channel restores the Reynolds number to its original value.

Observe that the flows with close to transition Reynolds numbers cross transition zones and exit with laminar Reynolds numbers. The simulations predict Reynolds number reductions from inlet to outlet of the hot vessel of 33 to 20 percent depending on the system pressure (higher reduction percentage at lower pressures).

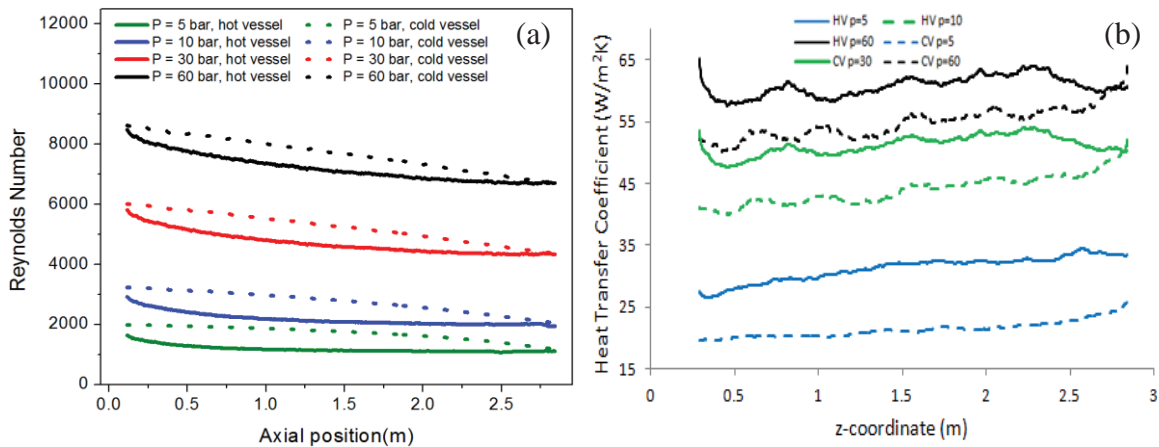


**Figure 15 a) Axial variations of Reynolds number for nitrogen under a range of system pressures (1 - 60 bar) displaying a full cycle as nitrogen passes through heated and cooled vessels b) Heat transfer coefficient in heated and cooled channels for various system pressures.**

Simulations displayed inlet Rayleigh numbers in the heated channel on the order of  $10^6$ . The Rayleigh number is defined as the product of Grashof and Prandtl numbers and the natural convection flows would be laminar if the Rayleigh number is below  $10^9$ . Thus, the simulations predicted mostly laminar nature of

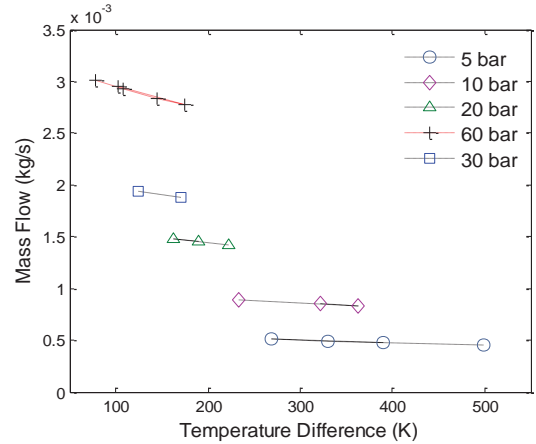


**Fig. 14 Effects of pressure and temperature difference between hot and cold vessels (or heater power) on natural circulation flow**

**Table 1. Role of natural circulation in heat dissipation**

Pressure (bar)	Input Power (W)	Heat Carried by Fluid (W)	Percentage (%)
60	3,275	990	30.2
30	3,085	774	25.1
10	2,825	455	16.1
5	2,725	239	8.8

the flows studied here.<sup>[23]</sup> Due to this nature, it is not surprising that the heat transfer coefficients in the heated and cooled channels were mostly constant except for at the outlet and inlet of the vessels. The heat transfer coefficient was also found to be a strong function of the system pressure (Fig. 15b). In addition, heat transfer coefficients in the heated channel were found to be higher than those in the cooled channel. This difference was a function of pressure; at lower pressures the difference between the heat transfer coefficients could be as much as 40% to as low as 10% for higher pressures.

#### 5.2.2.1 Effect of Heater Power

Of additional interest was the mass flux behavior in the closed flow loop and observing the parametric effects. Thus, a parametric study on the heater power was conducted, and the results were examined together with the pressure effect. These simulations were carried out for both DCC and PCC conditions. The total heater input power was varied from 1.5 to 6 kW to simulate the reduced reactor power under controlled, pressurized conditions. It was observed that at a given pressure as the heater power was increased and the temperature difference between the hot and cold vessels increased, the mass flux increased. As the heater power is increased in the hot vessel, the graphite temperature increases and fluid density decreases, so the hydrostatic head difference between the hot and cold vessels increases, resulting in a higher mass flux.

The heat transfer coefficient in the heated vessel was predicted to decrease as the heater power was reduced. This is as expected since the heat transfer coefficient is proportional to the bulk fluid temperature. As the total input power was decreased from 5,750 W to 2,500 W, the average heat transfer coefficient was predicted to decrease from 66 to 58 W/m<sup>2</sup>K. Similarly, from the parametric studies performed, it was observed that contrary to intuition, as the heater power is increased, the average Reynolds number decreases. As heater power is increased, average graphite and fluid temperatures increase, leading to an increase in the velocity. However, the fluid viscosity increases as well with temperature at a faster rate than the velocity. Thus, in natural circulation, the average Reynolds number in the hot channel would decrease due to an increase in fluid viscosity at higher input power levels.

## 6. CONCLUSIONS

Three-dimensional conjugate heat transfer and fluid flow calculations were performed for a single flow channel in a graphite test section in order to investigate the influence of several parameters on key phenomena related to degraded heat transfer in a VHTR such as flow laminarization. Forced convection simulations were successfully compared to experimental data and with several available correlations for validation. Parametric studies for various inlet Reynolds numbers were carried out using a standard  $k-\epsilon$  model. Natural circulation simulations were also performed for the experiment geometry using a laminar flow model. Based on the results obtained, the following conclusions can be drawn:

1. The results of the CFD calculations for forced convection of air showed significant reductions of up to 35% in Reynolds and Nusselt numbers between the test section inlet and outlet. The reductions in the Reynolds and Nusselt numbers are directly related to the strong variations in fluid properties with bulk fluid temperature, such as viscosity and thermal conductivity.
2. Based on the agreement seen between the experimental and numerical simulation results for forced convection, additional numerical studies were conducted for a two vessel configuration. Natural circulation flows are expected to occur in a VHTR under PCC and DCC conditions due to fluid temperature and density differences between the hot fuel zone and cooler reflector zone in the reactor core. Preliminary experiments using two graphite test sections showed the occurrence of natural circulation with heat transport taking place between the hot and cold vessels.
3. Numerical results displayed average temperature differences between hot and cold vessels of 573 K for a maximum graphite temperature of 923 K in the hot vessel. The simulations also predicted Reynolds number reductions from inlet to outlet of the hot vessel of 33 to 20 percent depending on the system pressure (higher reduction percentage at lower pressures). These simulations highlight the effective heat dissipating properties of VHTR reactors under accident scenarios.

4. The fluid flow model (laminar,  $k-\varepsilon$  and low Re  $k-\varepsilon$  turbulence models) used in numerical simulations had a minor impact on the Reynolds number predictions (<1.5% difference) but as much as a 15% difference in the Nusselt number predictions.

Future work includes further CFD model validation based on experimental data and carrying simulations for helium as the working fluid.

## ACKNOWLEDGMENTS

This work has been performed using a grant from the DOE Office of Nuclear Energy's Nuclear Energy University Program. The authors would like to thank Dr. Donald M. McEligot for assistance on data analysis and insight on the subjects presented in this paper.

## REFERENCES

1. Ball, S.J., and Fisher S.E., "Next-Generation Nuclear Plant (NGNP) Phenomena Identification and Ranking Table (PIRT) for Accident and Thermal Fluids Analysis," NUREG/CR-6944, 2007.
2. McEligot, D.M., and Banston, C.A., "Numerical Predictions for Circular Tube Laminarization by Heating," NASA Center, ASME Paper 69-HT-52, 1969.
3. Mikielewicz, D.P., Shehata, A.M., Jackson, J.D., and McEligot, D.M., "Temperature, velocity and mean turbulence structure in strongly heated internal gas flows: Comparison of numerical prediction with data," Int. J. Heat and Mass Transfer 45, 4333-4352, 2002.
4. Launder, B.E., "Laminarization of the turbulent boundary layer by acceleration", Technical Report 77, MIT Gas Turbine Lab, 1964.
5. Shehata, A.M., "Mean Turbulence Structure in Strongly Heated Air Flows," Ph.D. thesis, University of Arizona, Tucson, U.S.A., 1984.
6. Shehata, A.M. and McEligot, D.M., "Mean structure in the viscous layer of strongly heated internal gas flows. Measurements," Int. J. Heat Mass Transfer 41, 4297-4313, 1998.
7. Valentín, F. I., Artoun, N., Bindra, B., and Kawaji, M., "Investigation of flow Laminarization and Heat Transfer Reduction in a VHTR Reactor Core". Submitted to ANS Winter Meeting and Technology Expo - 2014, Anaheim, California, November 9-13, 2014.
8. COMSOL Multiphysics Reference Manual, Stockholm, Sweden, 2007.
9. Monarch Instrument. <http://www.monarchserver.com/TableofEmissivity.pdf> Web. 30 Jan. 2015.
10. Incropera, F.P., and Dewitt, D.P., Fundamentals of Heat and Mass Transfer, 5th ed., John Wiley & Sons, 2002.
11. Valentín, F.I., Artoun, N., Kawaji, M., and McEligot, D.M., "Experimental Study of forced convection heat transfer during upward and downward flow of helium at high pressure and high temperature," Submitted to ASTFE Engineering Summer Conference Expo- 2015, New York, August 9-12, 2015.
12. Holman, J.P., Heat Transfer, 9<sup>th</sup> ed., McGraw-Hill, New York, 2002.
13. McEligot, D.M., Shehata, A.M., Webster, N.Y., and Kunugi, T., "Prediction of strongly-heated gas flows," INEEL/CON--97-01336, 1997.
14. McEligot, D.M., Magee, P.M., and Leppert, G., "Effect of Large Temperature Gradient on Convective Heat Transfer: The Downstream Region," Journal of Heat Transfer, 87, 67-76, 1965.
15. Taylor, M.F., "Experimental Local Heat Transfer Data for Precooled Hydrogen and Helium at Surface Temperatures up to 5300 R," NASA-Lewis Research Center Technical Note TN D-2595, 1965.
16. Taylor, M.F., "Correlation of Local Heat-Transfer Coefficients for Single-Phase Turbulent Flow of Hydrogen in Tubes with Temperature Ratio of 23," NASA-Lewis Research Center Technical Note TN D-4332, 1967.
17. Dalle Donne, M. and Meerwald, E., "Experimental Local Heat-transfer and Average Friction Coefficients for Subsonic Turbulent Flow of Air in an Annulus at High Temperatures," Int. J. Heat Mass Transfer, 9, 1361-1376, 1966.
18. Dalle Donne, M. and Meerwald, E., "Heat-transfer and Friction Coefficients for Turbulent Flow of Air in smooth Annuli at High Temperatures," Int. J. Heat Mass Transfer, 19, 787-809, 1973.
19. Olson, D.A. and Grover, M.P., "Heat Transfer in a Compact Tubular Heat Exchanger with Helium Gas at 3.5 MPa," National Institute of Standards and Technology Report NISTIR 3941, 1990.
20. Travis, B.W. and El-Genk, M.S., "Numerical Simulation and Turbulent Convection Heat Transfer Correlation for Coolant Channels in a Very-High-Temperature Reactor," Heat Transfer Engineering, 34(1), 1-14, 2013.
21. W.B. Hall, J.D. Jackson, Laminarization of a turbulent pipe flow by buoyancy forces, ASME 69-HT-55, 1969.
22. McEligot, D.M., Coon, C.W., and Perkins, H.C., Relaminarization in tubes, Int. J. of Heat Mass Transfer 13 (1969) 431-433.
23. Bejan, A., Heat Transfer, Wiley, New York, 1993.